



**HAL**  
open science

## On the use of $^{17}\text{O}$ NMR for understanding molecular and silica-grafted tungsten oxo siloxide complexes

Y. Bouhoute, D. Grekov, N. Merle, K. Szeto, C. Larabi, I. del Rosal, L. Maron, L. Delevoye, R. Gauvin, M. Taoufik

### ► To cite this version:

Y. Bouhoute, D. Grekov, N. Merle, K. Szeto, C. Larabi, et al.. On the use of  $^{17}\text{O}$  NMR for understanding molecular and silica-grafted tungsten oxo siloxide complexes. *Dalton Transactions*, 2023, 52 (28), pp.9573-9581. 10.1039/D3DT01593A . hal-04238255

**HAL Id: hal-04238255**

**<https://hal.science/hal-04238255v1>**

Submitted on 12 Oct 2023

**HAL** is a multi-disciplinary open access archive for the deposit and dissemination of scientific research documents, whether they are published or not. The documents may come from teaching and research institutions in France or abroad, or from public or private research centers.

L'archive ouverte pluridisciplinaire **HAL**, est destinée au dépôt et à la diffusion de documents scientifiques de niveau recherche, publiés ou non, émanant des établissements d'enseignement et de recherche français ou étrangers, des laboratoires publics ou privés.

## On the use of $^{17}\text{O}$ NMR for the understanding of molecular and silica-grafted tungsten oxo siloxide complexes.

Y. Bouhoute,<sup>a</sup> D. Grekov,<sup>b</sup> N. Merle,<sup>b</sup> K. Szeto,<sup>a</sup> C. Larabi,<sup>a</sup> I. Del Rosal,<sup>c</sup> L. Maron,<sup>c</sup> L. Delevoye,<sup>b</sup> R. M. Gauvin,<sup>d</sup> M. Taoufik<sup>a,\*</sup>.

<sup>a</sup> Laboratoire de Chimie, Catalyse, Polymères et Procédés, UMR 5265 CNRS/ESCPE-Lyon/UCBL, ESCPE Lyon, F-308-43, Boulevard du 11 Novembre 1918, F-69616 Villeurbanne Cedex, France. E-mail : mostafa.taoufik@univ-lyon1.fr

<sup>b</sup> Univ. Lille, CNRS, Centrale Lille, Univ. Artois, UMR 8181 – UCCS – Unité de Catalyse et Chimie du Solide, Lille, F-59000, France.

<sup>c</sup> Laboratoire de Physico-Chimie des Nano-Objets, CNRS UMR 5215, Université de Toulouse, INSA, UPS, 135 Avenue de Rangueil, F-31077 Toulouse, France

<sup>d</sup> PSL Research University, Chimie ParisTech - CNRS, Institut de Recherche de Chimie Paris, 75005, Paris, France

*Abstract:*  $^{17}\text{O}$ -labelled tungsten siloxide complexes  $[\text{WOCl}_2(\text{OSi}^i\text{Bu}_3)_2]$  (**1-Cl**) and  $[\text{WOMe}_2(\text{OSiPh}_3)_2]$  (**1-Me**) were prepared and characterized by  $^{17}\text{O}$  MAS NMR, with input from theoretical calculations of NMR parameters. Guidelines linking  $^{17}\text{O}$  NMR parameters and coordination sphere of molecular and silica-grafted tungsten oxo species are proposed. The grafting of **1-Me** on  $\text{SiO}_{2-700}$  afforded material **2**, with surface species  $[(\equiv\text{SiO})\text{WOMe}_2(\text{OSiPh}_3)]$  as shown by elemental analysis, IR and  $^1\text{H}$  and  $^{13}\text{C}$  MAS NMR. DFT calculations of the grafting mechanism are in line with the observed reactivity. They indicate the occurrence of several isomeric species of close energy for the grafted W centers, precluding efficient  $^{17}\text{O}$  MAS NMR studies. Lack of catalytic reactivity studies in olefin metathesis and ring-opening olefin metathesis polymerization indicate that initiation by  $\alpha\text{-H}$

elimination is not operative in **2**, contrary to related tungsten surface species, which illustrates the crucial influence of the nature of the metal coordination sphere.

## Introduction

Tungsten oxide dispersed on silica, also known as the Phillips catalyst (not to be confused with the Cr/SiO<sub>2</sub> olefin polymerization Phillips catalyst), is used in several major industrial processes, due to its efficiency in olefin metathesis.<sup>1,2,3</sup> Beyond trial and error approach for its improvement, there is a major interest in investigating the nature of the active sites within this system, especially down to a molecular level. In particular, bis-siloxide oxo carbenic species [(≡SiO)<sub>2</sub>WO(CHR)] have been proposed as catalytically active sites.<sup>4</sup> Since our early works about 10 years ago on well-defined silica-grafted [WOR<sub>3</sub>(OSi≡)] species (R= CH<sub>2</sub>C(CH<sub>3</sub>)<sub>3</sub>),<sup>5</sup> the quest for models and alternatives to this ill-defined catalyst has motivated several studies, where variation of the ligands present in the coordination sphere of the metal was performed. **Examples of metathesis active silica-supported oxo carbenic species have been reported.**<sup>6</sup> **In addition,** thanks to proper design of the organometallic precursor, we have developed bisgrafted species [(≡SiO)<sub>2</sub>WO(CH<sub>2</sub>SiMe<sub>3</sub>)<sub>2</sub>] from grafting of [WO(CH<sub>2</sub>SiMe<sub>3</sub>)<sub>3</sub>Cl] onto silica dehydroxylated at 200 °C.<sup>7</sup> This species displayed very interesting catalytic properties, which motivated further investigation on related siloxide species. Indeed, in order to retain a similar tungsten coordination sphere, we chose in the present study to perform the grafting of the oxo bisalkyl bisiloxide complexes described by Wolczanski for oxo atom transfer reaction, namely of the type [WOR<sub>2</sub>(OSi<sup>*t*</sup>Bu<sub>3</sub>)<sub>2</sub>].<sup>8</sup> They feature a coordination sphere close to that postulated for the active centers in WO<sub>3</sub>/SiO<sub>2</sub>, and closely related to that of [(≡SiO)<sub>2</sub>WO(CH<sub>2</sub>SiMe<sub>3</sub>)<sub>2</sub>]. More precisely, we considered using the silox<sup>9</sup> derivative [WOMe<sub>2</sub>(OSi<sup>*t*</sup>Bu<sub>3</sub>)<sub>2</sub>] (**1-Me**) as a precursor for the design of silica-supported precatalysts for olefin metathesis. We therefore proceeded to study the reactivity of **1-Me** towards partially dehydroxylated silica. Furthermore, bearing in mind the high potential of solid state NMR to investigate the molecular structure of (supported) organometallic



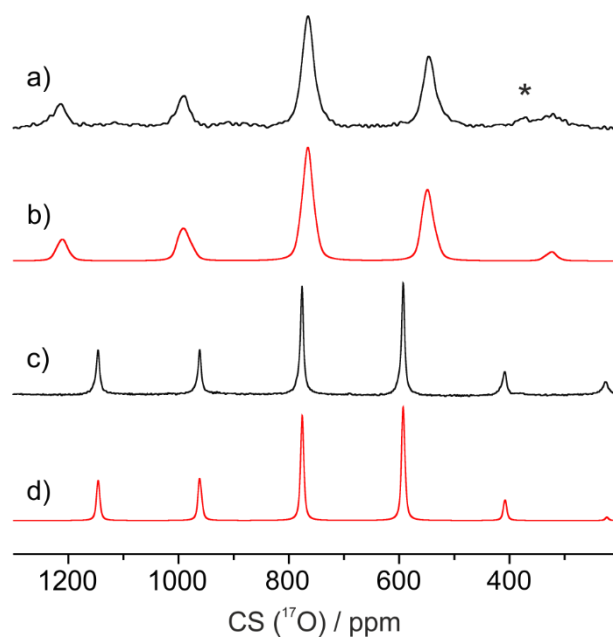


**Figure 1.**  $^{17}\text{O}$  MAS NMR spectra of **1-Cl** at a) 9.4 and c) 18.8 T, along with the corresponding best-fit simulations, b) and d), respectively. Spectra recorded at 9.4 and 18.8 T were acquired with 10000 and 4000 transients, and MAS rates were set at 12 and 20 kHz, respectively.

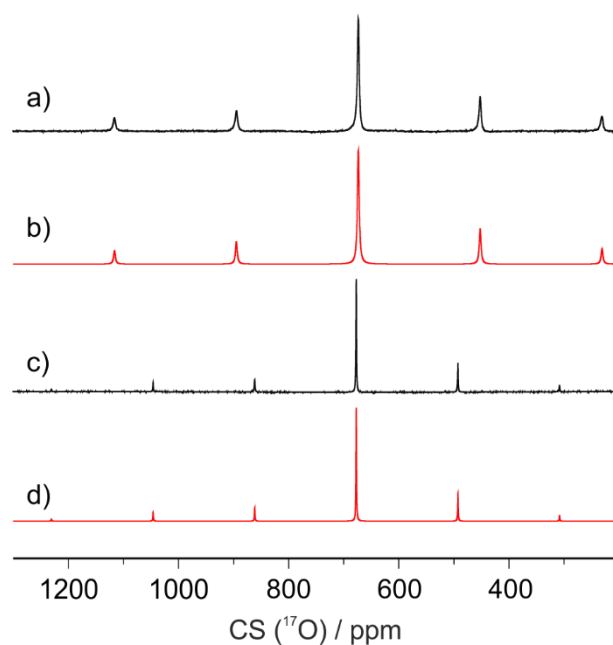


**Figure 2.**  $^{17}\text{O}$  MAS NMR spectra of **1-Me** at a) 9.4 and c) 18.8 T, along with the corresponding best-fit simulations, b) and d), respectively. Spectra recorded at 9.4 and 18.8 T were acquired with 1024 and 512 transients, and MAS rates were set at 12 and 20 kHz, respectively.

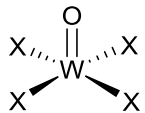
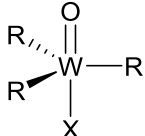
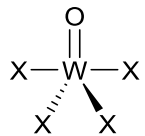
Isotropic and anisotropic parameters were deduced from best-fit simulations for both **1-Cl** and **1-Me**, (Table 1). Regarding the isotropic chemical shift (CS), both values are in line with those previously obtained for similar high-valent tungsten species bearing terminal oxo moieties.<sup>7,1618</sup> The line shapes are characteristic of <sup>17</sup>O sites featuring low quadrupolar coupling constants and moderate chemical shift anisotropies. The chloride derivative features a higher CS value than its alkyl counterpart, in line with the electron-withdrawing effect from the halide ligands, compared to the  $\sigma$ -donating alkyl substituents. Regarding the anisotropic parameters, such as the quadrupolar coupling constant, a higher value was determined for **1-Cl** compared to that of **1-Me** (2.7 and 0.15 MHz, respectively). Comparison with DFT calculated values showed that chemical shift and quadrupolar coupling constant are well in line with experimental data (Table 1). This is not so much the case for the chemical shift anisotropy, or for the asymmetry parameters, which may differ significantly.

**Table 1.** Experimental and calculated <sup>17</sup>O NMR parameters for **1-Cl** and **1-Me**

Species		CS (ppm)	C <sub>Q</sub> (MHz)	$\eta_Q$	$\Delta_{CSA}$	$\eta_{CSA}$
1-Cl	exp.	782 ( $\pm 2$ )	2.7 ( $\pm 0.2$ )	0.5 ( $\pm 0.2$ )	555 ( $\pm 10$ )	0.2 ( $\pm 0.1$ )
	calc.	769	2.9	0.4	789	0.9
1-Me	exp.	675 ( $\pm 2$ )	0.2 ( $\pm 0.2$ )	0.2 ( $\pm 0.1$ )	270 ( $\pm 30$ )	0.2 ( $\pm 0.2$ )
	calc.	655	0.36	0.7	456	0.3

These sets of <sup>17</sup>O NMR parameters for the terminal oxo species can be compared to that of the WOR<sub>3</sub>X derivative. Whereas compounds **1-Cl** and **1-Me** adopt a trigonal bipyramidal configuration with the oxo in the trigonal plane, the trisalkyl species feature a square pyramidal configuration with an apical position for the oxo functionality. We can then propose a classification for terminal oxo species, depending on the geometry.

**Table 2.** Structure - NMR parameters relationships for oxo species (error margins are omitted for the sake of clarity)

Species	CS (ppm)	C <sub>Q</sub> (MHz)	Δ <sub>CSA</sub> (ppm)	Ref.	
[WOCl <sub>4</sub> ]	671	1.0	-330	16	
	[(≡SiO) <sub>2</sub> WOCl <sub>3</sub> ]	828	<1.3	-350	16
	[(≡SiO)WOCl <sub>2</sub> ]	810	<2.0	-640	16
	[(≡SiO)WO(CH <sub>2</sub> CMe <sub>3</sub> ) <sub>3</sub> ]	757	5.3	-1136	18
	[(≡SiO)WO(CH <sub>2</sub> SiMe <sub>3</sub> ) <sub>3</sub> ]	774	5.2	-1110	19
	[(≡SiO) <sub>2</sub> WO(CH <sub>2</sub> SiMe <sub>3</sub> ) <sub>2</sub> ]	766	5.5	-1062	7
	[WOCl(CH <sub>2</sub> CMe <sub>3</sub> ) <sub>3</sub> ]	735	5.1	-1110	18
	[WO{OSi(O <i>t</i> Bu) <sub>3</sub> }(CH <sub>2</sub> CMe <sub>3</sub> ) <sub>3</sub> ]	731	5.44	-1128	18
	[O(WO(CH <sub>2</sub> CMe <sub>3</sub> ) <sub>3</sub> )]	775	4.6	-1112	18
	[WOCl <sub>2</sub> (OSi <i>t</i> Bu <sub>3</sub> ) <sub>2</sub> ] ( <b>1-Cl</b> )	782	2.7	555	This work
	[WOMe <sub>2</sub> (OSi <i>t</i> Bu <sub>3</sub> ) <sub>2</sub> ] ( <b>1-Me</b> )	675	0.2	270	This work

Over the scope of structures studied by <sup>17</sup>O NMR, chemical shift values are observed within the 828-675 ppm range. Noteworthy, though [WOCl<sub>4</sub>] has a CS value in the lower range, care should be taken as in the solid-state structure this compound consists of chains of tungsten species interacting via coordination of the oxo moiety.<sup>16</sup> The oxo function is therefore not to be considered as purely terminal in this compound. When comparing structurally related species, for instance and [WOCl(CH<sub>2</sub>CMe<sub>3</sub>)<sub>3</sub>] and [WO{OSi(O*t*Bu)<sub>3</sub>}(CH<sub>2</sub>CMe<sub>3</sub>)<sub>3</sub>], the substitution of a chloride by a siloxide has only a minor influence on the CS value (735 and 731 ppm, respectively).

In order to shed light on the significant difference in the chemical shift values of **1-Cl** and **1-Me**, a natural chemical shielding (NCS) analysis<sup>20</sup> has been performed on the corresponding DFT models (Figure 3).

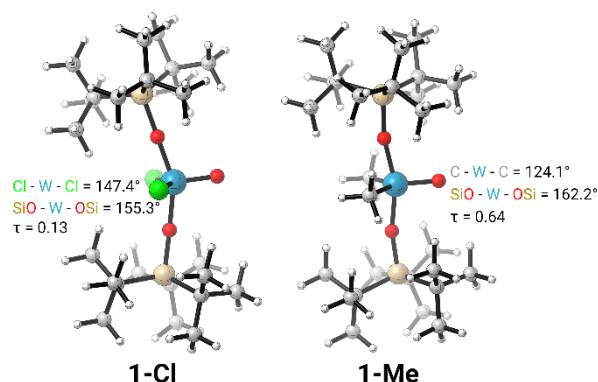


**Figure 3.** DFT Optimized structures of **1-Cl** and **1-Me** and selected angles.

As we can see on Figure 4, for **1-Cl**, the most deshielded component ( $\delta_{11}/\sigma_{11}$ ) is on the plane containing the three oxygen atoms and perpendicular to the W-O bond. The intermediate component ( $\delta_{22}/\sigma_{22}$ ) is also perpendicular to the W-O bond, but lies in the plane containing the two chlorides and the terminal oxo, while the most shielded component ( $\delta_{33}/\sigma_{33}$ ) is oriented along the W-O bond perpendicular to the two other components. For **1-Me**, the positions of components  $\delta_{11}$  and  $\delta_{22}$  are interchanged while that of  $\delta_{33}$  remains along the W-O bond. Further analysis of the individual components of the chemical shift tensor reveals that this large deshielding of **1-Cl** compared to **1-Me** is associated to a highly deshielded  $\delta_{11}$  component (1295 ppm vs. 959 ppm). The  $\delta_{22}$  and  $\delta_{33}$  components are quite similar for both complexes.

Thanks to the NCS analysis, this most deshielded component  $\delta_{11}/\sigma_{11}$  can be decomposed into diamagnetic ( $\sigma_{\text{dia}}$ , leading to shielding) and paramagnetic ( $\sigma_{\text{para}}$ , leading in general to deshielding) terms. As we can see on Figure 4, the  $\sigma_{\text{dia}}$  term is similar in both complexes (around 400 ppm). The diamagnetic term mainly comes from the 1s core orbitals of the oxygen atoms which causes shielding of the nucleus. Since the core orbitals are insensitive to the local molecular structure, it is not surprising to find the same values for **1-Cl** and **1-Me**. In contrast, the  $\sigma_{\text{para}}$  term differs strongly between the two complexes. The individual orbital contributions to the  $\delta_{11}/\sigma_{11}$  component for **1-Cl** and



**1-Me** reveals that in both cases this large deshielding is caused by a coupling of the  $\sigma(\text{W-O})$  orbital with the low-lying vacant  $\pi^*(\text{W-O})$  orbital, as also observed for  $^{13}\text{C}$  NMR calculations.<sup>21</sup> Thus, the higher deshielding of **1-Cl** compared to **1-Me** originates from the lower energy gap between the  $\sigma$ - and  $\pi^*$  orbitals for **1-Cl**, principally due to the stabilization of LUMO orbitals (see Figure S3 in Supporting Information).

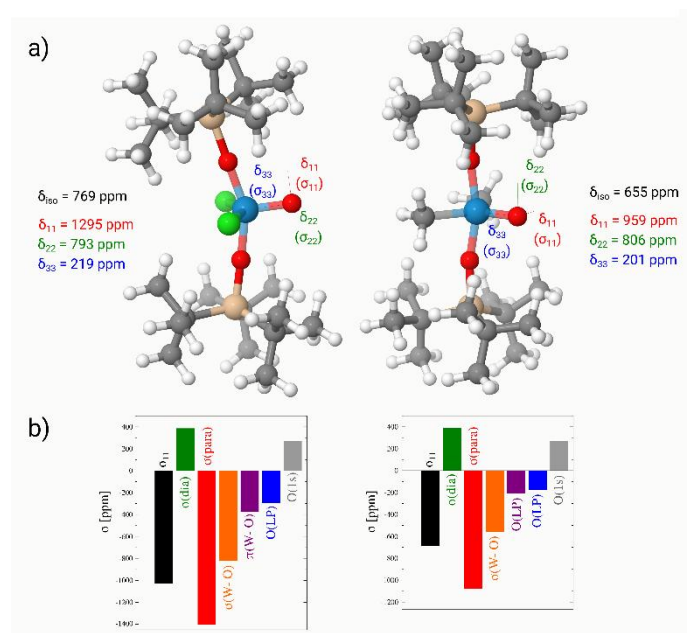


**Figure 4.** a) Orientation of the chemical shielding tensor in **1-Cl** and **1-Me** and b) results of the NCS analysis for the principal components of the chemical shielding tensor of **1-Cl** (left) and **1-Me** (right).

When considering the quadrupolar coupling constant for complexes featuring an oxo moiety in apical position, the geometry of the considered species has a major, clear-cut impact: square pyramidal configuration gives rise to values significantly lower than those of trigonal bipyramidal ones (respectively [1.0 — < 2] MHz and [4.6 — 5.5] MHz range). This tendency is also observed for the chemical shift anisotropy, which is most particularly high in the case of the trigonal bipyramidal species (-1062 — -1136 ppm), resulting in the very characteristic signal manifold for such species.<sup>18,19</sup> In the case of **1-Cl** and **1-Me**, in the absence of single crystal X-ray diffraction study, one may rely on DFT-optimized structure for geometry assessment (Figure 3). Both compounds feature a configuration analogous to that of the bis *n*-butyl derivative  $[\text{WO}(n\text{-Bu})_2(\text{OSi}t\text{Bu}_3)_2]$ , namely of distorted trigonal

bipyramidal type, with the oxo and alkyl groups in the meridional positions. Significant differences between the two computed structures are observed, most particularly regarding the SiO-W-OSi and X-W-X angles (X= Cl, CH<sub>3</sub>, Figure 3). These values can be used to calculate the  $\tau$  parameter, which is a descriptor for assessment of pentacoordinated complex geometry distinguishing between square pyramidal ( $\tau = 0$ ) and trigonal bipyramidal geometry ( $\tau = 1$ ).<sup>22</sup> Complex **1-Cl** features a  $\tau$  value of = 0.13, thus being close to square pyramidal, while **1-Me** yields a  $\tau$  value of = 0.64, thus leaning toward a trigonal bipyramidal configuration. For comparison, the  $\tau$  value is of 0.57 in [WO(*n*-Bu)<sub>2</sub>(OSi*t*Bu<sub>3</sub>)<sub>2</sub>]. Thus, the impact of these distinct geometries for **1-Cl** and **1-Me** is a significant difference in quadrupolar coupling constant (respectively of 2.7 and 0.16 MHz). Interestingly, DFT-calculated  $C_Q$  value for isolated molecules of [WOCl<sub>4</sub>] (of square pyramidal geometry) is 1.8 MHz, comparable to the experimental value of **1-Cl**. This illustrates how this anisotropic parameter can be a better descriptor than isotropic chemical shift, when characterizing terminal oxo species. Moreover, it also demonstrates the advantage of relying on solid-state MAS rather than on liquid state NMR spectroscopy, as it provides anisotropic parameters, as illustrated by the study on a series of vanadium oxo derivatives featuring alkyl and siloxide groups, where <sup>17</sup>O chemical shift tendency falls short of providing structural information.<sup>23</sup>

As discussed above, the grafting of such species is interesting when aiming at preparing high-valent oxo tungsten (pre-)catalysts for olefin metathesis, that can be probed as models for the industrial Phillips catalyst's active sites. Immobilization of **1-Me** may proceed via distinct pathways, such as the W-C or W-O silanolysis. If surface silanols react with W-Me or W-OSi*t*Bu<sub>3</sub> moieties, this affords respectively [(≡SiO)WOMe(OSi*t*Bu<sub>3</sub>)<sub>2</sub>] (with methane release) or [(≡SiO)WOMe<sub>2</sub>(OSi*t*Bu<sub>3</sub>)] (with *t*Bu<sub>3</sub>SiOH release). The silica used as a support in this case is Aerosil 200 from Evonik, which was partially dehydroxylated under vacuum at 700 °C (SiO<sub>2-700</sub>). This material features a specific area of 190 m<sup>2</sup>.g<sup>-1</sup>, and a SiOH surface density of 0.7 OH.nm<sup>-2</sup>. The residual silanol groups are non-interacting, as evidenced by the characteristic sharp signal at 3747 cm<sup>-1</sup> on the infrared spectrum (Figure 5a).

**1-Me** was reacted with  $\text{SiO}_{2-700}$  at room temperature in pentane, affording material **2** as a pale-yellow powder. Gas phase analysis showed no trace of methane released in the grafting process. Elemental analysis indicates W and C loadings of 3.31 and 3.71 w%, which correspond to 17 C/W within the material. This is in line with the formation of  $[(\equiv\text{SiO})\text{WOMe}_2(\text{OSi}t\text{Bu}_3)]$  (15 C/W), resulting from  $\text{HOSi}t\text{Bu}_3$  release. This silanol compound was indeed observed by  $^1\text{H}$  NMR analysis of the supernatant liquid from the grafting reaction. The tungsten loading is lower than that of related materials, such as 4.02 w% for  $[(\equiv\text{SiO})\text{WO}(\text{CH}_2t\text{Bu})_3]$ , for instance. This latter compound results from the grafting of  $\text{WOCl}(\text{CH}_2t\text{Bu})_3$  on  $\text{SiO}_{2-700}$ , which proceeds with full silanol consumption. Thus, the silanol reaction is unlikely to be complete in the case of **1-Me** grafting, most probably due to the severe steric hindrance from the  $\text{OSi}t\text{Bu}_3$  groups. The uncomplete  $\text{SiOH}$  consumption is confirmed by IR studies indicating partial consumption of the silanols (Figure 5b). The non-interacting silanol signal at  $3747\text{ cm}^{-1}$  is mostly absent from the IR spectrum of **2**, and weak, broad bands resulting from interacting silanols are observed at  $3692$  and  $3490\text{ cm}^{-1}$  (the latter being very broad). It results most probably from  $\text{SiO-H}$  perturbed by grafted organometallic centers. Accordingly,  $\nu(\text{C-H})$  bands are also observed in the  $2990\text{-}2880\text{ cm}^{-1}$  range.

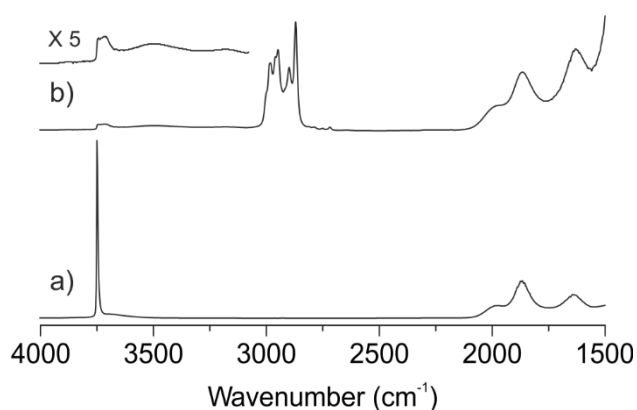


**Figure 5.** DRIFTS spectra of a)  $\text{SiO}_{2-700}$  and b) **2**

The  $^1\text{H}$  MAS NMR spectrum of **2** (Figure 6) features a signal at 1.3 ppm, which accounts for both  $\text{Si}t\text{Bu}$  and  $\text{WMe}$  protons. This is in line with the 1.19 ppm chemical shift for the *t*-butyl groups in **1-Me**. As the  $\text{W-Me}$  groups in **1-Me** give rise to a  $^1\text{H}$  NMR signal at 1.65 ppm ( $\text{C}_6\text{D}_6$ ), the

corresponding signal in **2** is most probably located as a shoulder on the *t*Bu peak. The  $^{13}\text{C}$  CP MAS NMR spectrum (Figure 6) comprises 3 signals, at 49.0, 28.5 and 23.5 ppm. These respectively account for W-Me (47.0 ppm in **1-Me**) and primary and quaternary carbons from Si/*t*Bu groups (30.1 and 24.1 ppm in **1-Me**).

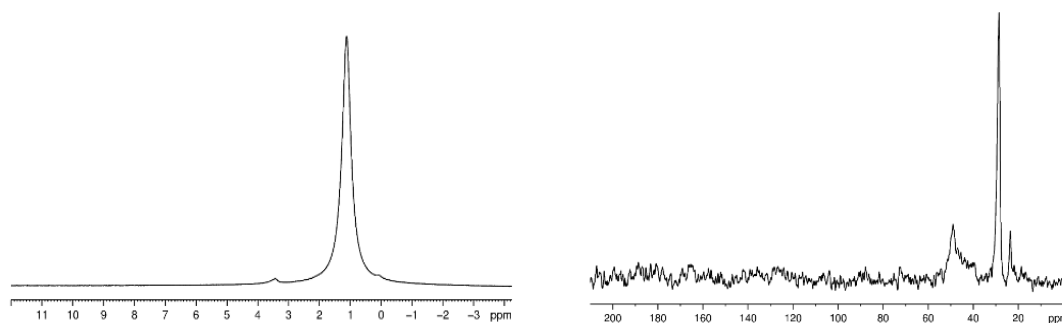


**Figure 6.**  $^1\text{H}$  (left) and  $^{13}\text{C}$  CP (right) MAS NMR spectra of **2** (11.75 T, spinning speed 10 kHz)

The W-oxo moiety within  $^{17}\text{O}$ -labelled **2-Me** proved challenging to observe by  $^{17}\text{O}$  MAS NMR, requiring an extended acquisition time. The oxo moiety gives rise to a series of broad, featureless peaks, with a maximum intensity in the isotropic signal at about 720 ppm (Figure 7a). A tentative best fit simulation can be proposed, thanks to the relative intensities within the W=O peaks manifold (Figure 7b). The corresponding NMR parameters are a chemical shift of 730 ( $\pm 3$ ) ppm, a quadrupole coupling constant of 4.0 MHz ( $\pm 0.5$ ), and  $\Delta_{\text{CSA}}$  of 500 ( $\pm 50$ ) ppm. Both the chemical shift and quadrupole coupling constant are significantly higher than that of the molecular precursor **1-Me**, (respectively 675 ppm and 0.2 MHz), which hints at a distinct configuration around the metal center between **2** and **1-Me**.

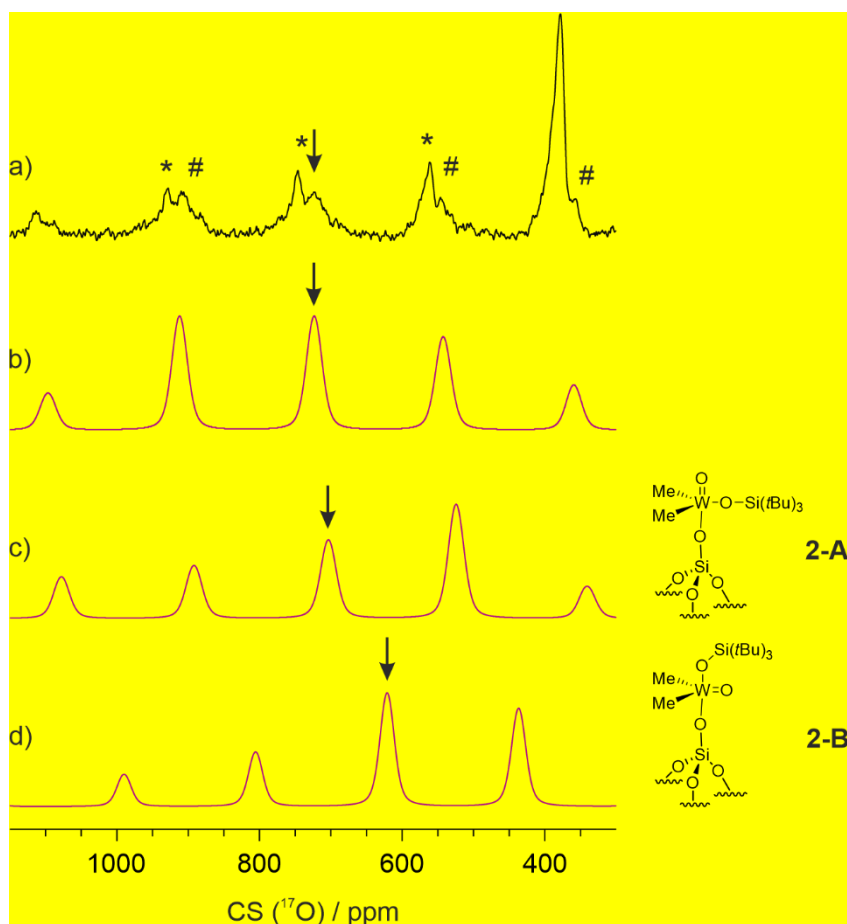


**Figure 7.** a)  $^{17}\text{O}$  MAS NMR spectrum of **2** at 18.8 T, with arrow designating the isotropic chemical shift of the WO moiety signals and # for the spinning side bands (\*:  $\text{ZrO}_2$  rotor signal, 240000 transients), b) best fit simulation of  $^{17}\text{O}$  MAS NMR signal of W=O in **2**, and c), d) and e) simulated  $^{17}\text{O}$  MAS NMR spectrum of W=O within DFT models for surface species (arrow: isotropic chemical shift).

In order to gain a better understanding on the grafting reaction of **1-Me** onto  $\text{SiO}_{2-700}$ , the enthalpy profile for this reaction was computed at the DFT level (B3PW91). The isolated silanols groups onto the  $\text{SiO}_{2-700}$  surface were modeled using a molecular polyoligosilsesquioxane complex, as successfully used in previous studies.<sup>7,18,24</sup> Two different reaction pathways have been computed (Figure 8): either (i) the W- $\text{CH}_3$  silanolysis with the concomitant methane release or (ii) the W- $\text{OSi}t\text{Bu}_3$  silanolysis leading to the release of  $\text{HOSi}t\text{Bu}_3$ . The W- $\text{CH}_3$  silanolysis, as can be seen in the blue and green profiles are kinetically accessible (21.4 and 18.3 kcal mol<sup>-1</sup>) and thermodynamically very favorable (-36.5 and -37.7 kcal mol<sup>-1</sup>). This barrier is lower (by 7 kcal mol<sup>-1</sup>) for the W- $\text{OSi}t\text{Bu}_3$  silanolysis, as

can be seen in the black and red profiles, due to a better charge distribution at the transition state. However, It is also noteworthy that, from a thermodynamic point of view, the formation of  $[(\equiv\text{SiO})\text{WOMe}(\text{OSi}t\text{Bu}_3)_2]$  is more favorable than that of  $[(\equiv\text{SiO})\text{WOMe}_2(\text{OSi}t\text{Bu}_3)]$  ( $\sim 37$  vs  $\sim 9.5$  kcal.mol<sup>-1</sup>). Thus, calculations suggest that  $[(\equiv\text{SiO})\text{WOMe}_2(\text{OSi}t\text{Bu}_3)]$  is the kinetic product of the grafting reaction, while  $[(\equiv\text{SiO})\text{WOMe}(\text{OSi}t\text{Bu}_3)_2]$  is the thermodynamic one.

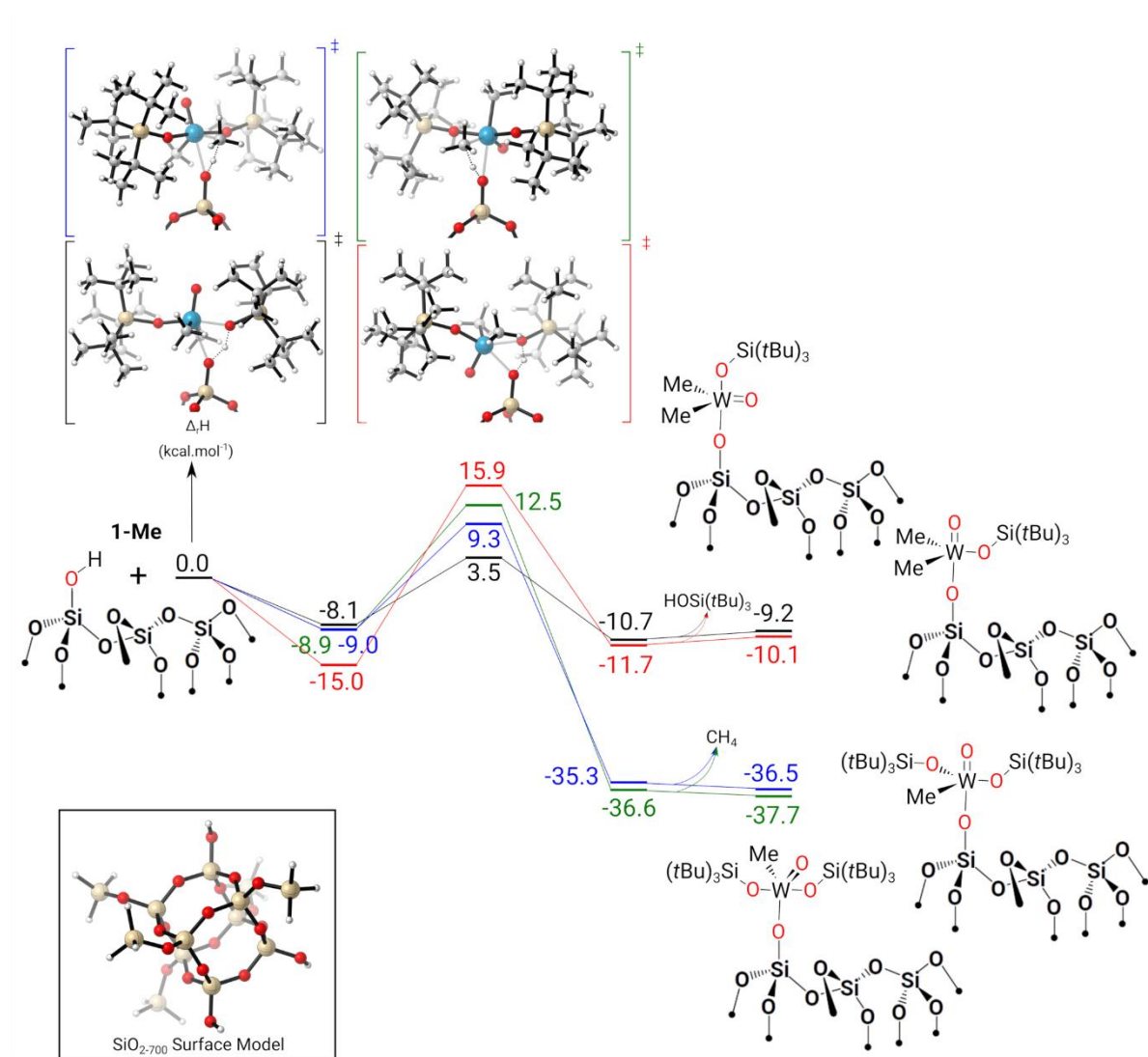


**Figure 8.** Calculated enthalpy profiles of the different pathways of the grafting of **1-Me** onto  $\text{SiO}_2\text{-700}$

DFT calculations have shown that  $[(\equiv\text{SiO})\text{WOMe}_2(\text{OSi}t\text{Bu}_3)]$  can feature two isomeric structures which are very close in energy, depending on the ligand in *trans* position from the surface siloxide (either the oxo or the silox ligand). The interconversion barrier of 8.4 kcal.mol<sup>-1</sup> between these two isomeric structures show that they can coexist within material **2** (see Figure S4). Calculation of the <sup>17</sup>O

NMR features of the oxo moiety in the *trans*-oxo (**2A**) and the *trans*-siloxide (**2B**) species indicates that these present chemical shift within the same range (717 and 621 ppm, respectively) while the quadrupolar coupling constant is significantly affected by the change in geometry (4.2 and 0.3 MHz, respectively) (See Table S1). Simulated  $^{17}\text{O}$  MAS NMR spectra of the two DFT models are displayed on Figure 7 (c for **2A** and d for **2B**). Thus, if interconversion occurs rapidly under the measurement conditions, it is expected that the  $^{17}\text{O}$  NMR signal manifold will be significantly affected. It has been reported by Schurko *et al.* that if an exchange occurs between two states of non-equal ground state energies, the resulting NMR lineshape will most likely be heavily weighted to the lowest energy conformer and would be minimally affected by motions.<sup>25</sup> In the present case, based on the isotropic chemical shift of the WO moiety in **2** estimated at about 730 ppm, it is more likely that the major configuration of the surface species is that of DFT model **2A**, namely with the oxo function in *trans* position to the surface siloxide.

Bis-alkyl complex **1-Me** is thermally stable, that is, despite the *cis* arrangement of the two alkyl groups, they do not undergo  $\alpha$ -H elimination to generate an alkylidene function.<sup>8</sup> This is most probably due to the insufficient steric pressure within the dimethyl species, hindering the process.<sup>26</sup> However, we also observed previously that  $[(\equiv\text{SiO})\text{WO}(\text{CH}_2\text{ECH}_3)_3]$  (E= C, Si) do not afford alkylidene complexes upon heating, but generate carbene species in the presence of the olefinic substrate, as metathesis is initiated under such conditions. Thus, it seemed relevant to probe the reactivity of **2** toward olefins. We first attempted to perform propene metathesis in batch reactor, based on our previous results with group 6 oxo pre-catalysts. However, no conversion of propene was observed even upon heating at 80°C for 10 hours. We thus probed the reactivity of **2** towards a less demanding substrate such as norbornene. Indeed, oxo alkyl species were previously shown to be able to initiate the ring opening metathesis polymerization of this monomer.<sup>27</sup> There again, no activity was detected, both for the molecular **1-Me** and the supported **2**. Nevertheless, this lack of activity in metathesis nicely illustrates the importance of the coordination sphere geometry: Indeed, species featuring an oxo-bisalkyl-bissiloxide set of ligands but with a different geometry (square pyramidal) than that of **2**

(presumably trigonal bipyramidal from DFT calculations) display high activity in propene metathesis, due to a more efficient initiation into catalytically-active carbene species.

## Conclusion

Tungsten oxo siloxide species were probed as precatalysts for olefin metathesis, in the view of mimicking postulated active sites in industrial catalysts. Use of  $^{17}\text{O}$  solid state NMR helped in linking spectroscopic and structural features for coordination and organometallic WO derivatives, with the support of theoretical calculations. Grafting of such a derivative was studied via a joint experimental and spectroscopic study. We demonstrated that selective grafting occurs by siloxide ligand protonolysis, affording a bisalkyl species. While the supported material proved inactive towards linear and cyclic olefinic substrates, this contribution illustrates how the design of catalysts is of prime importance in the development of efficient catalytic systems, as can be mediated via ligand sphere modifications.<sup>28</sup>

## Experimental section

All experiments were carried out by using standard Schlenk and glovebox techniques. Solvents were purified and dried according to standard procedures.  $\text{C}_6\text{D}_6$  (SDS) was distilled from NaK and stored in glovebox. **1-Cl** and **1-Me** were synthesized following the literature procedure.<sup>8</sup>  $^{17}\text{O}$ -enriched  $\text{WOCl}_4$  was prepared using the reported method using 90 %  $^{17}\text{O}$ -labelled water from Cortecnet.<sup>16</sup>  $\text{SiO}_{2-700}$  was prepared from Aerosil silica (Degussa, specific area of  $200 \text{ m}^2 \text{ g}^{-1}$ ), which was dehydroxylated at  $700^\circ\text{C}$  under high vacuum ( $10^{-5}$  Torr) for 15 h to give a white solid having a specific surface area of  $190 \text{ m}^2 \text{ g}^{-1}$  and containing  $0.7 \text{ OH nm}^{-2}$ . Elemental analyses were performed at the Pascher Mikroanalytisches Labor at Remagen-Bandorf (Germany). IR spectra were recorded on a Nicolet 6700 FT-IR spectrometer by using a DRIFT cell equipped with  $\text{CaF}_2$  windows. The samples were prepared under argon within a glovebox. Typically, 64 scans were accumulated for each spectrum (resolution  $4 \text{ cm}^{-1}$ ).



**NMR Characterization.** Solution NMR spectra were recorded on an Avance-300 Bruker spectrometer. All chemical shifts were measured relative to residual  $^1\text{H}$  or  $^{13}\text{C}$  resonances in the deuterated solvent:  $\text{C}_6\text{D}_6$ ,  $\delta$  7.15 ppm for  $^1\text{H}$ , 128 ppm for  $^{13}\text{C}$ .  $^1\text{H}$  and  $^{13}\text{C}$  solid-state MAS NMR spectra were recorded on Bruker Avance-500 and Bruker Avance-300 spectrometers with a conventional double-resonance 4 mm CP MAS probe at the Laboratoire de Chimie Organométallique de Surface. The samples were introduced under argon in a zirconia rotor (4 mm), which was then tightly closed. In all experiments, the rotation frequency was set to 10 kHz unless otherwise specified. Chemical shifts were given with respect to TMS as external reference for  $^1\text{H}$ ,  $^{13}\text{C}$  and  $^{29}\text{Si}$  NMR. The  $^{17}\text{O}$  solid-state NMR spectra were acquired on a Bruker Avance II 400 ( $^1\text{H}$ , 400.13 MHz;  $^{17}\text{O}$ , 54.27 MHz) and Avance III 800 ( $^1\text{H}$ , 800.13 MHz,  $^{17}\text{O}$ , 108.47 MHz) spectrometers, using a single pulse sequence (Avance II 400 : pulse excitation of 5  $\mu\text{s}$  at an RF field strength of 60 kHz, Avance III 800: pulse excitation of 4  $\mu\text{s}$  at an RF field strength of 60 kHz) and 3.2 mm rotor diameter. No proton decoupling was applied. The recycle delay was 0.5 sec.

**Preparation and characterization of 2.** A mixture of finely ground **1-Me** [ $\text{WOMe}_2(\text{OSi}t\text{Bu}_3)_2$ ] (134 mg, 0.203 mmol) and  $\text{SiO}_{2-200}$  (545 mg) was stirred at 40 °C (5 h) under dynamic vacuum whilst all volatile compounds were condensed into a cold trap. Pentane was then added and the solid was washed 5 times. The resulting yellow powder was dried under vacuum ( $10^{-5}$  Torr) and transferred to a 500 mL Schlenk tube in order to quantify methane evolved during grafting. The powder was then dried at 25 °C under static vacuum for 1 h. Analysis of the gas phase by gas chromatography indicated the formation of only traces of  $\text{CH}_4$  during the grafting. Elemental analysis: W 3.31 % wt; C 3.71 % wt.

**Simulation of  $^{17}\text{O}$  MAS NMR spectra.** All  $^{17}\text{O}$  MAS NMR numerical spectra were calculated using SOLA module included in TopSpin software package, using Haeberlen chemical shift tensor convention.

**DFT Methodological Details.** All DFT calculations were carried out with the Gaussian 09 suite of programs.<sup>29</sup> Geometries were fully optimized in gas phase without symmetry constraints, employing the B3PW91 functional.<sup>30,31</sup> The nature of the extrema was verified by analytical frequency calculations. The calculation of electronic energies and enthalpies of the extrema of the potential

energy surface (minima and transition states) were performed at the same level of theory as the geometry optimizations. IRC calculations were performed to confirm the connections of the optimized transition states. Stuttgart effective core potentials and their associated basis set were used for silicon and tungsten.<sup>32</sup> The basis sets were augmented by a set of polarization functions ( $\zeta_d = 0.284$  for Si and  $\zeta_f = 0.823$  for W).<sup>33</sup> For the other elements (H, C, Cl and O), Pople's double- $\zeta$  basis set 6-31G(d,p) was used.<sup>34</sup> The optimized structures were used for  $^{17}\text{O}$  NMR calculations. These calculations were also performed using a higher Dunning's correlation consistent basis set cc-PVTZ for the oxygen atoms.<sup>35</sup> In all cases, among the various theories available to compute shielding tensors, the Gauge Including Atomic Orbital (GIAO) method has been adopted for the numerous advantages it presents.<sup>36</sup> Typically, in order to compare our calculations with experimental values,  $^{17}\text{O}$  shielding has been converted to chemical shift using the usual equation:  $\delta_{\text{iso}} = \sigma_{\text{iso ref}} - \sigma_{\text{iso sample}}$ , where  $\sigma_{\text{iso ref}}$  is the isotropic  $^{17}\text{O}$  shielding of the liquid water. In the continuation of our previous studies,<sup>7,18</sup> an internal reference is used for the calibration of the  $\sigma_{\text{iso ref}}$  value:  $\sigma_{\text{iso ref}} = 292.2$  ppm. The  $^{17}\text{O}$  quadrupolar coupling constant  $C_Q$  and the asymmetry parameter  $\eta_Q$ , which describes the interaction between nuclear quadrupole moment of the oxygen nuclei with the electric field gradient (EFG) arisen at these sites, are calculated from the EFG tensor eigenvalues  $V_{11}$ ,  $V_{22}$ , and  $V_{33}$ . The NCS–NBO analysis<sup>37</sup> allows a quantitative partitioning of the isotropic shielding constants of each nucleus for which GIAO calculations were performed, showing the Lewis “L” and non-Lewis “NL” contributions arising from each occupied NBO as well as the analysis of the shielding tensor in terms of canonical MOs, following Ditchfield's original treatment.

### **Authors contribution**

Y. B.: investigation; D. G.: investigation, writing, N. M.: investigation, K. S.: investigation, C. L.: investigation, I. D. R.: investigation, writing, L. M.: investigation, writing, L. D.: supervision, writing, R. M. G.: supervision, writing – original draft, M. T.: supervision, conceptualization, writing.

### **Conflict of interest**

No conflict of interest to declare.

## Acknowledgement

This work was principally financed by the Agence Nationale de la Recherche (ANR-12-BS07-0021-01, OXOCAT). The CNRS, French Ministry of Research and Higher Education, Institut de chimie de Lyon, Chevreul Institute (FR 2638), Région Nord-Pas de Calais, and FEDER are acknowledged for their supplementary support. Financial support from the IR-RMN-THC FR 3050 for conducting the research is gratefully acknowledged. L.M. is member of the Institut Universitaire de France. This work was performed using HPC resources from CALMIP (Grant 2016-p0833).

## References

- 1 S. Lwin, I. E. Wachs, *ACS Catal.* **2014**, *4*, 2505-2520.
- 2 J.C. Mol, *J. Molec. Catal. A* **2004**, *213*, 39-45.
- 3 N. Popoff, E. Mazoyer, J. Pelletier, R. M. Gauvin, M. Taoufik, *Chem. Soc. Rev.*, **2013**, *42*, 9035-9054.
- 4 W. Grunert, R. Feldhaus, K. Anders, E. S. Shpiro, K. M. Minachev, *J. Catal.* **1989**, *120*, 444-456.
- 5 E. Mazoyer, N. Merle, A. de Mallmann, J.-M. Basset, E. Berrier, L. Delevoye, J.-F. Paul, C. P. Nicholas, R. M. Gauvin, M. Taoufik, *Chem. Commun.* **2010**, *46*, 8944-8946.
- 6 (a) M. P. Conley, V. Mougél, D. V. Peryshkov, W. P. Forrest, D. Gajan, A. Lesage, L. Emsley, C. Copéret, R. R. Schrock, *J. Am. Chem. Soc.* **2013**, *135*, 19068-19070; (b) M. Pucino, V. Mougél, R. Schowner, A. Fedorov, M. R. Buchmeiser, C. Copéret, *Angew. Chem. Int. Ed.* **2016**, *55*, 4300-4302.
- 7 Y. Bouhoute, D. Grekov, N. Merle, K. C. Szeto, A. De Mallmann, F. Lefebvre, G. Raffa, I. Del Rosal, L. Maron, R. M. Gauvin, L. Delevoye, M. Taoufik, *ACS Catal.*, **2016**, *6*, 1-18
- 8 D. C. Rosenfeld, D. S. Kuiper, E. B. Lobkovsky, P. T. Wolczanski, *Polyhedron*, **2006**, *25*, 251-258
- 9 P. T. Wolczanski, *Chem. Commun.*, **2009**, 740-757.
- 10 D. Grekov, T. Vancompernelle, M. Taoufik, L. Delevoye, R. M. Gauvin, *Chem. Soc. Rev.* **2018**, *47*, 2572 - 2590.
- 11 N. Merle, J. Trébosc, A. Baudouin, I. Del Rosal, L. Maron, K. Szeto, M. Genelot, A. Mortreux, M. Taoufik, L. Delevoye, R. M. Gauvin, *J. Am. Chem. Soc.* **2012**, *134*, 9263-9275

- 
- 12 I. P. Gerothanassis, *Prog. Nucl. Magn. Reson. Spectrosc.*, **2010**, *56*, 95-197.
- 13 S. E. Ashbrook, M. E. Smith, *Chem. Soc. Rev.*, **2006**, *35*, 718-735.
- 14 S. E. Ashbrook, Z. H. Davis, R. E. Morris, C. M. Rice, *Chem. Sci.*, **2021**, *12*, 5016-5036.
- 15 T.-X. Métro, C. Gervais, A. Martinez, C. Bonhomme, D. Laurencin, *Angew. Chem. Int. Ed.*, **2017**, *56*, 6803-6807.
- 16 Y. Bouhoute, A. Garron, D. Grekov, N. Merle, G. Girard, N. Popoff, A. De Mallmann, I. Del Rosal, L. Maron, R. M. Gauvin, L. Delevoye, M. Taoufik, *ACS Catal.*, **2014**, *4*, 4232-4241.
- 17 V. C. Gibson, T. P. Kee, A. Shaw, *Polyhedron* **1988**, *7*, 579-580
- 18 N. Merle, G. Girard, N. Popoff, A. De Mallmann, Y. Bouhoute, J. Trébosc, E. Berrier, J.-F. Paul, I. Del Rosal, L. Maron, R. M. Gauvin, L. Delevoye, M. Taoufik, *Inorg. Chem.* **2013**, *52*, 10119-10130.
- 19 D. Grekov, Y. Bouhoute, K. C. Szeto, N. Merle, A. De Mallmann, F. Lefebvre, I. Del Rosal, L. Maron, R. M. Gauvin, L. Delevoye, M. Taoufik, *Organometallics*, **2016**, *35*, 2188-2196.
- 20 (a) J. A. Bohmann, F. Weinhold, T. C. Farrar, *J. Chem. Phys.* **1997**, *107*, 1173-1184; (b) J. Autschbach, *J. Chem. Phys.* **2008**, *128*, 164112; (c) J. Autschbach, S. Zheng, *Magn. Reson. Chem.* **2008**, *46*, S45-S55; (d) F. Aquino, B. Pritchard, J. Autschbach, *J. Chem. Theory Comput.* **2012**, *8*, 598-609.
- 21 (a) C. Gordon, K. Yamamoto, K. Searles, S. Shirase, R. A. Andersen, O. Eisenstein, C. Copéret, *Chemical Science*, **2018**, *9*, 1912-1918; (b) C. P. Gordon, S. Shirase, K. Yamamoto, R. A. Andersen, O. Eisenstein, C. Copéret, C. NMR chemical shift analysis decodes olefin oligo- and polymerization activity of d 0 group 4 metal complexes, *Proc. Natl. Acad. Sci.* **2018**, *115*, E5867-E5876; (c) C. P. Gordon, K. Yamamoto, W.-C. Liao, F. Allouche, R. A. Andersen, C. Copéret, C. Raynaud, O. Eisenstein, *ACS Cent. Sci.* **2017**, *3*, 759-768; (d) C. P. Gordon, C. Copéret, *Chimia*, **2019**, *73*, 252-256.
- 22 A. W. Addison, T. N. Rao, J. Reedijk, J. van Rijn, G. C. Verschoor *J. Chem. Soc., Dalton Trans.*, **1984**, 1349-1356.
- 23 F. J. Feher, R. L. Blanski *Organometallics*, **1993**, *12*, 958
- 24 (a) I. del Rosal, I. C. Gerber, R. Poteau, L. Maron, *J. Phys. Chem. A*, **2010**, *114*, 6322-6330; (b) I. del Rosal, I. C. Gerber, R. Poteau, L. Maron, *New J. Chem.* **2015**, *39*, 7703-7715; (c) T. Vancompernelle, N. Merle, F. Capet, I. Del Rosal, M. Laurent, L. Delevoye, F. Pourpoint, R. M. Gauvin, *Dalton Trans.* **2019**, *48*, 5243-5252; (d) I. Del Rosal, S. Lassalle, C. Dinoi, C. Thieuleux, L. Maron, C. Camp, *Dalton Trans.* **2021**, *50*, 504-510.
- 25 R. W. Schurko, S. Wi, L. Frydman, *J. Phys. Chem. A* **2002**, *106*, 1, 51-62

---

26 R. R. Schrock, C. Copéret, *Organometallics*, **2017**, *36*, 1884–1892

27 C. Larabi, K. C. Szeto, Y. Bouhoute, M. O. Charlin, N. Merle, A. De Mallmann, R. M. Gauvin, L. Delevoye, M. Taoufik, *Macromol. Rapid. Commun.*, **2016**, *37*, 1832-1836.

28 Y. Bouhoute, D. Grekov, N. Merle, K. Szeto, I. Del Rosal, L. Maron, L. Delevoye, R. M. Gauvin, M. Taoufik, *Catal. Sci. Tech.*, **2016**, *6*, 8532-8539.

<sup>29</sup> Gaussian 09, Revision D.01, M. J. Frisch, G. W. Trucks, H. B. Schlegel, G. E. Scuseria, M. A. Robb, J. R. Cheeseman, G. Scalmani, V. Barone, G. A. Petersson, H. Nakatsuji, X. Li, M. Caricato, A. Marenich, J. Bloino, B. G. Janesko, R. Gomperts, B. Mennucci, H. P. Hratchian, J. V. Ortiz, A. F. Izmaylov, J. L. Sonnenberg, D. Williams-Young, F. Ding, F. Lipparini, F. Egidi, J. Goings, B. Peng, A. Petrone, T. Henderson, D. Ranasinghe, V. G. Zakrzewski, J. Gao, N. Rega, G. Zheng, W. Liang, M. Hada, M. Ehara, K. Toyota, R. Fukuda, J. Hasegawa, M. Ishida, T. Nakajima, Y. Honda, O. Kitao, H. Nakai, T. Vreven, K. Throssell, J. A. Montgomery, Jr., J. E. Peralta, F. Ogliaro, M. Bearpark, J. J. Heyd, E. Brothers, K. N. Kudin, V. N. Staroverov, T. Keith, R. Kobayashi, J. Normand, K. Raghavachari, A. Rendell, J. C. Burant, S. S. Iyengar, J. Tomasi, M. Cossi, J. M. Millam, M. Klene, C. Adamo, R. Cammi, J. W. Ochterski, R. L. Martin, K. Morokuma, O. Farkas, J. B. Foresman, D. J. Fox, Gaussian, Inc., Wallingford CT, 2016.

<sup>30</sup> A. D. Becke, *J. Chem. Phys.* **1993**, *98*, 5648-5652

<sup>31</sup> J. P. Perdew, J. A. Chevary, S. H. Vosko, K. A. Jackson, M. R. Pederson, D. J. Singh, C. Fiolhais, *Phys.Rev. B* **1992**, *46*, 6671-6687.

<sup>32</sup> A. Bergner, M. Dolg, W. Kuechle, H. Stoll, H. Preuss, *Mol. Phys.* **1993**, *80*, 1431 – 1441.

<sup>33</sup> A. W. Ehlers, M. Böhme, S. Dapprich, A. Gobbi, A. Höllwarth, V. Jonas, K. F. Köhler, R. Stegmann, A. Veldkamp, G. Frenking, *Chem. Phys. Lett.* **1993**, *208*, 111-114.

<sup>34</sup> a) R. Ditchfield, W. J. Hehre, J. A. Pople, *J. Chem. Phys.* **1971**, *54*, 724-728; b) W. J. Hehre, R. Ditchfield, J. A. Pople, *J. Chem. Phys.* **1972**, *56*, 2257-2261; c) P. C. Hariharan, J. A. Pople, *Theor. Chim. Acta* **1973**, *28*, 213-222; d) M. M. Francl, W. J. Pietro, W. J. Hehre, J. S. Binkley, M. S. Gordon, D. J. DeFrees, J. A. Pople, *J. Chem. Phys.* **1982**, *77*, 3654-3665.

<sup>35</sup> a) E. R. Davidson, *Chem. Phys.* **1996**, *260*, 514; b) D. E. Woon, T. H. Dunning, *J. Chem. Phys.* **1993**, *98*, 1358.

<sup>36</sup> a) K. Wolinski, J. F. Hilton, P. Pulay, *J. Am. Chem. Soc.* **1990**, *112*, 8251; b) 41 R. McWeeny, *Phys Rev.* **1962**, *126*, 1028; c) F. J. London, *Phys. Radium* **1937**, *8*, 397 ; d) 43 J. L. Dodds, R. McWeeny, A. J. Sadlej, *Mol.*

---

*Phys.* **1980**, *41*, 1419; e) R. Ditchfield, *Mol. Phys.* **1974**, *27*, 789; f) P. C. Junk, J. W. Steed, *J. Organomet. Chem.* **1999**, *587*, 191.

<sup>37</sup> **NBO 7.0**. E. D. Glendening, J. K. Badenhoop, A. E. Reed, J. E. Carpenter, J. A. Bohmann, C. M. Morales, P. Karafiloglou, C. R. Landis, F. Weinhold, Theoretical Chemistry Institute, University of Wisconsin, Madison (2018).